4. CONCLUSIONS

Slot-type SRR as a new perturbation element in dual-mode square patch filter is introduced for the first time. Dual-mode filter using square patch resonator embedded slot-type SRR is presented and analyzed. Then, an improved dual-mode filter using square patch with two notches and slot-type SRR is designed and fabricated. Measured results show that the designed structure exhibits the insertion loss of less than 1 dB, 3-dB bandwidth of 7.9%, and two transmission zero near the passband. Because of its advantages of low loss, compact size, high selectivity, and no high degenerate mode near the passband, it has great applications in RF circuits and system.

ACKNOWLEDGMENTS

The authors thank State Key Laboratory of Millimeter Wave for fund support (Grant No.: K200907).

REFERENCES

1. L.H. Hsieh and K. Chang, Dual-mode elliptic-function bandpass filter using one single patch resonator without coupling gaps, Electron Lett 36 (2000), 2022–2023.
2. L. Zhu, P.M. Wecowski, and K. Wu, New planar dual-mode filter using cross-slotted patch resonator for simultaneous size and loss reduction, IEEE Trans Microwave Theory Tech 47 (1999), 650–654.
3. Y. Sung, Compact and low insertion loss dual-mode bandpass filter, Microwave Opt Technol Lett 50 (2008), 3201–3206.
4. Y. Sung, B.Y. Kim, C.S. Ahn, and Y.-S. Kim, Compact and low-insertion-loss dual-mode patch filter with spur-lines, Microwave Opt Technol Lett 43 (2004), 33–34.
5. O. Akgun, B.S. Tezekici, and A. Gorur, Reduced-size dual-mode slotted patch resonator for low-loss and narrowband bandpass filter applications, Electron Lett 40 (2004), 1275–1277.
6. J.B. Pendry, A.J. Holden, D.J. Robbins, and W.J. Stewart, Magnetism from conductors and enhanced nonlinear phenomena, IEEE Trans Microwave Theory Tech MTT-47 (1999), 2075–2084.
7. D.R. Smith, W.J. Padilla, D.C. Vier, S.C. Nemat-Nasser, and S. Schultz, Composite medium with simultaneously negative permeability and permittivity, Phys Rev Lett 84 (2000), 4184–4187.
8. J. Martel, J. Bonache, R. Marqués, F. Martín, and F. Medina, Design of wide-band semi-lumped bandpass filters using open split ring resonators, IEEE Microwave Wireless Compon Lett 17 (2007), 28–30.
9. J.-D. Tseng and W.-G. Chang, Planar rectangular split ring shape bandpass structures, Microwave Opt Technol Lett 49 (2007), 2520–2523.
10. S.-H. Fu and C.-M. Tong, A novel CSRR-based defected ground structure with dual-bandgap characteristics, Microwave Opt Technol Lett 51 (2009), 2908–2910.
11. N.-I. Jo, D.-O. Kim, and C.-Y. Kim, A compact band notched UWB antenna for mobile applications, PIERS Online 2010, 177–180.
12. J.S. Hong and M.J. Lancaster, Microstrip filters for RF/microwave application, Wiley, New York, NY, 2001.

NOVEL MICROWAVE FILTERS BASED ON EPSILON NEAR ZERO WAVEGUIDE TUNNELS

Alonso Corona-Chavez, D. V. B Murthy, and Jose Luis Olvera-Cervantes
Department of Electronics, National Institute of Astrophysics, Optics and Electronics (I.N.A.O.E), Puebla-72840, Mexico;
Corresponding author: alonsocorona@inaoep.mx

Received 27 October 2010

ABSTRACT: *Microwave filters based on the concept of Epsilon Near Zero (ENZ) tunneling effect are presented. ENZ metamaterials provide interesting phenomena such as anomalous tunneling and energy squeezing through ultra narrow waveguide channels. Using this concept two filters are demonstrated with Chebyshev response and one with a quasi-elliptic response by adding transmission zeroes with hairpin resonators. Experimental and simulated responses are presented with good agreement.* © 2011 Wiley Periodicals, Inc. Microwave Opt Technol Lett 53:1706–1710, 2011; View this article online at wileyonlinelibrary.com. DOI 10.1002/mop.26147

Key words: *epsilon near zero; metamaterials; microwave filters*

1. INTRODUCTION

In this article, the use of Epsilon Near Zero (ENZ) waveguide tunnels for narrow-band filter applications is proposed. ENZ metamaterials at microwave frequencies consist of metalo-dielectric structures in which the phase constant β of the propagating wave becomes zero at a particular frequency [1, 2]. This phenomenon, also known as supercoupling or tunneling, has caught much attention for microwave circuits due to the unique properties it provides [1–6]. Several ways have been previously proposed to achieve β=0 behavior. One of them is by using composite right left handed lines (CRLH) operated between their left and right hand propagation [7–9]. However, for filter applications, these structures have large radiation losses due to their fast-wave characteristic [9].

Another alternative to achieve β=0 is to use rectangular waveguides operated at the cutoff frequency of the TE_{10} mode [1]. Moreover, in [10], this phenomenon is achieved by loading a rectangular waveguide with complementary split ring resonators (CSRR).

As it has been shown in [11], the effective permittivity ε_{eff} of a rectangular waveguide operated at the TE_{10} mode can be described by Eq. (1)

$$\frac{\varepsilon_{\mathrm{eff}}}{\varepsilon_{\mathrm{o}}\varepsilon_{\mathrm{r}}} = n^2 - \frac{C^2}{4\varepsilon_r f^2 W_t^2} \tag{1}$$

where ε_r is the relative permittivity of the filling material, n is the refractive index of the filling material, c is the speed of light in vacuum, W_t is the waveguide width, and f is the operating frequency. From this equation, it is observed that the effective permittivity is zero at cutoff. Therefore, the propagation constant is also zero (β=0) leading to infinite wavelength and infinite phase velocity. Furthermore, when $\varepsilon_{\mathrm{eff}} \approx 0$ the wave follows a static-like behavior that allows reflection-less propagation [3–5].

In this work, this phenomenon is exploited to make miniaturized tunnels for filter applications in which the tunnel length can be made arbitrarily small as β=0. Also, since the tunnels are implemented on waveguide, there are no radiation losses as opposed to CRLH zeroth order resonators. Additionally, by using rectangular waveguide structures operated at their cutoff frequency, no extra CSRR loading is necessary.

In this article, two and three pole filters are designed with Chebyshev characteristic. Moreover, by adding two transmission zeros by means of hairpin resonators, a quasi-elliptic response is achieved. Simulated and experimental results are presented with good agreement.

2. EPSILON NEAR ZERO TUNNEL

As discussed in the previous section, an ENZ tunnel can be made as a conventional waveguide operated at the cutoff frequency of the TE_{10} mode. Therefore, its width W_t can be obtained from Eq. (2)

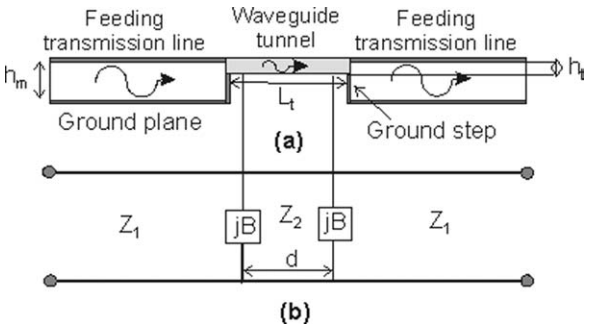

Figure 1 (a) ENZ tunnel; (b) equivalent circuit

$$W_t = \frac{c}{2 f_0 \sqrt{\varepsilon_r}} \tag{2}$$

where f_0 is the tunneling frequency, c is the speed of light, and ε_r is the relative permittivity. Figure 1(a) shows an ENZ tunnel, where the feeding lines consist of a top signal line and a ground plane (such as microstrip or parallel plate). If a large step exists between the feeding line and the narrow tunnel, such that $h_m >> h_t$, then the circuit can be modeled as shown in Figure 1(b) [12], where the narrow waveguide region can be replaced by a region having an effective length d and an impedance $Z_2=(h_t/h_m)Z_1$ [10]. Here, Z_1 is the impedance of the feeding lines. In addition, there is a shunt admittance $Y=jB$ between the mismatched waveguides that accounts for the step discontinuity. To calculate the reflection coefficient, Eq. (3) may be used as shown in [10]

$$\Gamma = \frac{\Gamma_2 \cdot (1 - e^{j2\beta_t L_t})}{1 - \Gamma_2 e^{j2\beta_t L_t}} \tag{3}$$

where $\Gamma_2 = (Z_2 \| Y - Z_1)/(Z_2 \| Y + Z_1)$ and $Z_2 \| Y = (-jB\ Z_2)/(-jB + Z_2)$. Since $h_m >> h_t$ then $Z_2 << Z_1$. Therefore, the reflection coefficient is very large, except for the case when $\beta=0$, which corresponds to the tunneling effect, when the reflection coefficient disappears.

To simulate the ENZ tunnel, two microstrip transmission lines are selected to feed the waveguide. The substrate has a relative permittivity of $\varepsilon_r=2.2$ with $tan\delta=0.001$. The height of the ENZ waveguide is chosen to be $h_t=0.5$mm and the height of the microstrip feed line $h_m=3.2$mm. The width of the tunnel is $W_t=30$mm, calculated for $f_0=3.5$ GHz. As discussed earlier, the tunnel length (L_t) can be arbitrarily small; however, due to manufacturing restrictions, we chose a length of 10 mm (equivalent to about $\lambda/6$ in an $\varepsilon_r=2.2$ medium at 3.5 GHz). Care should be taken when choosing L_t, since when $L_t = \lambda/2$, a conventional resonance is excited which could interfere with our tunneling frequency as explained in [5].

The width of the microstrip line is $W_m = 10$ mm corresponding to 50Ω. A 17.5 μm thick copper is used for all metallizations. To measure its unloaded quality factor (Q_0), an eigenmode simulation was performed in [13], giving a $Q_0 = 195$.

Moreover, the tunnel was fed by a capacitive gap with $A = 2$ mm as shown in Figure 2(a), and the simulation results shown in Figure 2(b), where the resonant frequency is $f_0 = 3.445$ GHz. The E-Field distribution is depicted in Figure 2, where it is clearly seen that at the tunneling frequency, the field is constant along the propagation direction x, proving the tunneling behavior.

3. CHEBYSHEV FILTER DESIGN

To prove the concept of using ENZ tunnels for narrow band filters, two filters were designed with Chebyshev responses. In this case, we consider narrow-band to be about 20% or less [14]. However, the bandwidth (BW) limitation is bound to manufacturing constraints, where wide-band filters require strong couplings between resonators and low external Q values which are difficult to achieve in planar photolithographic processes [15]. On the other hand, for filters with extremely narrow bands, technologies with higher unloaded Q values should be adopted [16].

The first circuit consists of a two pole Chebyshev filter with a frequency of operation $f_0 = 3.5$ GHz and a fractional BW of 12%. From [17], the low pass element g parameters are obtained for a 0.1 dB ripple as $g_o = g_3 = 1$ and $g_1 = g_2 = 0.75$. Then, from Eqs. (4) and (5), the required external coupling Q_{ext} and the resonator coupling k are obtained.

$$Q_{ext\,1} = \frac{g_0 \cdot g_1}{\Delta \mathrm{FEB}} = 6.3 = Q_{ext\,2} \tag{4}$$

$$k = \frac{\Delta \mathrm{FEB}}{\sqrt{g_1 \cdot g_2}} = 0.13 \tag{5}$$

where δFBW is the 3 dB frequency BW.

To calculate the external coupling (Q_{ext}), full wave simulations are carried out using the structure shown in Figure 3. In the figure, it is seen that one ENZ resonator is placed between two microstrip feed lines, where one of them is weakly coupled by means of a capacitive coupling gap $A = 1$ mm and a microstrip line of $W_{m2} = 0.5$ mm. The external coupling depends on the width of the microstrip line W_m, which was varied in a range from 0.5 mm to 10 mm. The external coupling was

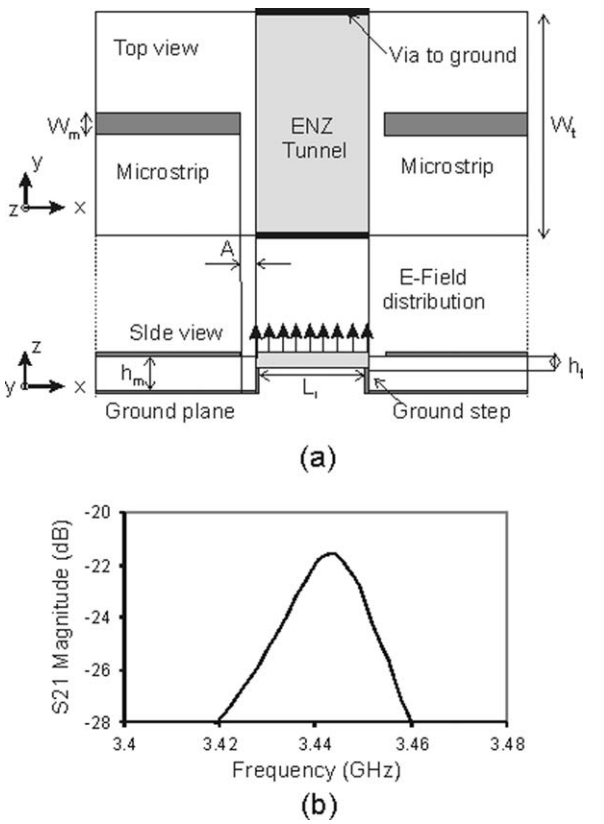

Figure 2 (a) Weakly coupled ENZ tunnel with E-Field distribution, (b) Response of weakly coupled ENZ tunnel

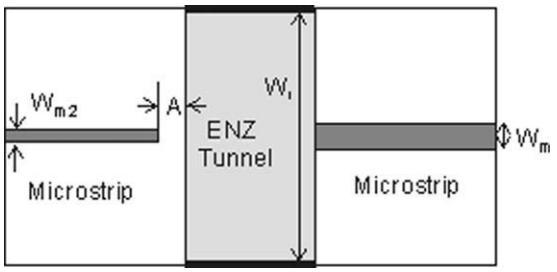

Figure 3 ENZ tunnel used to calculate external Q

obtained from Eq. (6) [14], where Δ*FBW* is the 3 dB frequency BW and f_0 is the center frequency. Figure 4 plots the different external quality factors versus the width of the microstrip line.

$$Q_{\text{ext 1}} = \frac{f_0}{\Delta FBW} \tag{6}$$

To calculate the coupling between contiguous tunnels, the structure in Figure 5 is simulated in [13]. Two microstrip lines of width $W_m = 6$ mm weakly couple two ENZ resonators through a capacitive gap $A = 0.5$ mm. The resonators are interconnected with a microstrip line of dimensions W_i and L. Two mechanisms can alter the k parameter. The first one is the width W_i and the second is length L. In this case, the width was left constant ($W_i = 10$ mm), and the length L was varied from 4 mm to 12 mm. The k value was extracted from Eq. (7) [14].

$$k = \frac{f_2^2 - f_1^2}{f_2^2 + f_1^2} \tag{7}$$

where f_1 and f_2 are the corresponding resonant frequencies seen from the simulated results. Figure 4 plots the k values vs. different line lengths.

The filter was modeled in a full wave simulator with the dimensions calculated from Figure 4. Then it was fine-tuned and the final dimensions are: $W_m = 6$ mm, $W_i = 10$ mm, $h_m = 3.2$ mm, $h_t = 0.5$ mm, $L = 9$ mm.

The second Chebyshev filter consists of a three-pole filter at the same center frequency and a fractional BW of 13%.

From [17], the low pass element g parameters are obtained as $g_0 = g_4 = 1$, $g_1 = g_3 = 0.6291$, and $g_2 = 0.9702$. Then, from Eqs. (4) and (5), the required external coupling Q_{ext} and the resonator coupling k are obtained as $Q_{ext} = 4.8$ and $k = 0.166$. From Figure 4, the dimensions of the filter can be calculated. Finally, the filter was fined tuned in the full wave simulator. The final dimensions are: $W_m = 10$ mm, $W_i = 10$ mm, $L = 8$ mm.

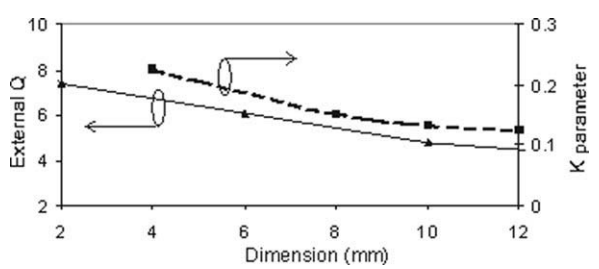

Figure 4 External quality factor Q_{ext} and k parameter vs. width of microstrip line (W_m) and length of interconnecting line (L), respectively

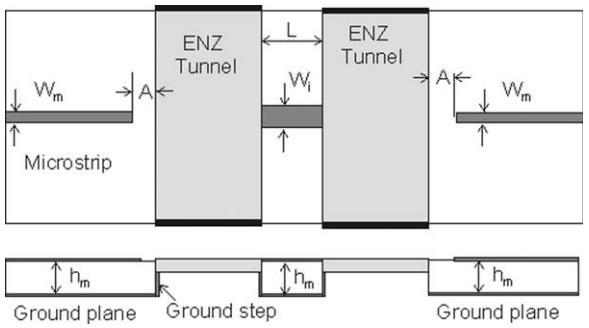

Figure 5 Structure used to calculate coupling k

Both filters are shown in Figure 6.

4. QUASI ELLIPTIC FILTER DESIGN

To enhance the roll-off response of the filters, two transmission zeroes were added at the edge of the passband of the 3-pole filter. This was done by means of hairpin resonators coupled to the feeding transmission line [18]. If the resonators were coupled to the tunnel interconnecting lines, the k values may be affected. Each resonator is dedicated to add a transmission notch at a particular frequency; hence for two notches at both ends of the passband, two resonators are required. The hairpin structure consists of a metallic inductive ring with a dielectric capacitive gap (also called split ring resonator). With proper design of the ring and gap, we can design an LC resonator at the required frequency. The split ring resonators are designed to resonate at 3.05 GHz and 4.2 GHz to have transmission zeros at each side of the band. The dimensions of the resonators are $a = 11.5$ mm, $c = 8.5$ mm with a gap $g = 1$ mm as shown in Figure 6. The electric response of the resonator can be controlled by adjusting the orientation of its gap with respect to the applied electric E field. The parameters that affect the resonator response are the shape, orientation, and the arrangement. The position of the split ring resonator is optimized by using [13]. Several simulations have been performed at different positions i.e., at the input port, output port, and between waveguides. The optimized positions of the hairpin resonator are shown in Figure 7.

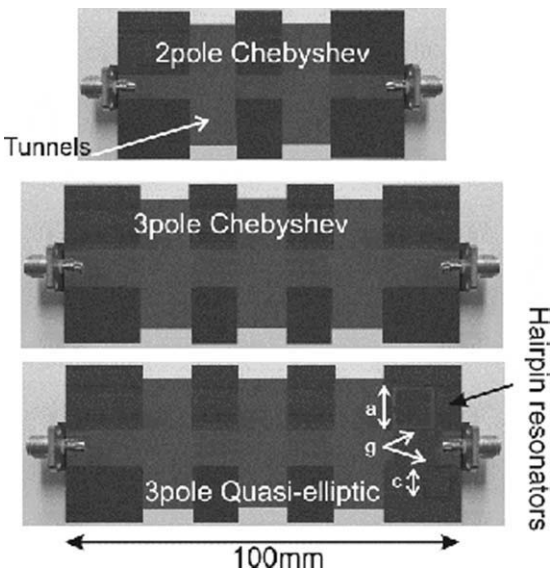

Figure 6 Final layout of 2-pole and 3-pole Chebyshev filters with ENZ tunnels along with quasi-elliptic filter with hairpin resonators

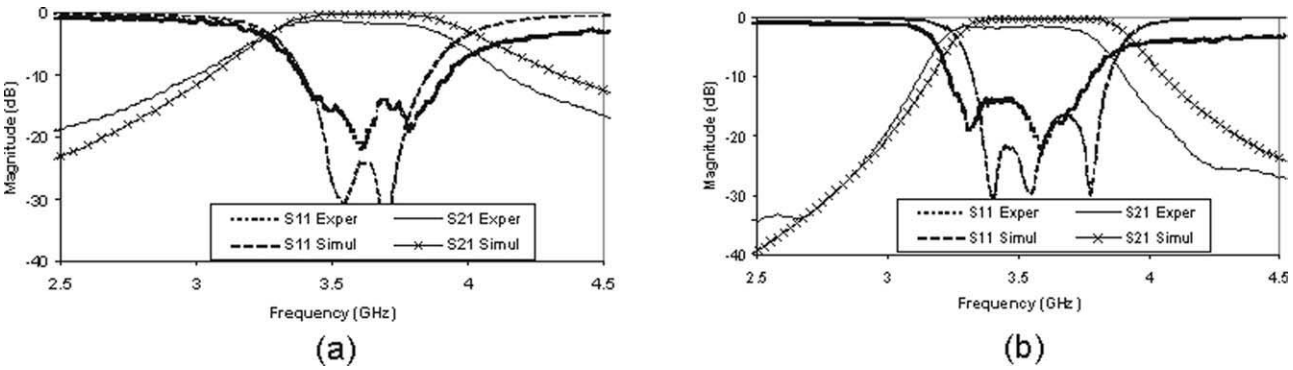

Figure 7 Simulated and experimental responses of (a) ENZ two-pole filter, (b) ENZ three-pole filter

5. SIMULATION AND EXPERIMENTAL RESULTS

All filters were implemented on a single piece of Rogers 5010 Duroid with $\varepsilon_r = 2.2$ and height $h = 3.2$ mm. To fabricate the tunnels, a standard PCB milling machine was utilized to carve down the substrate to the required tunnel height of 0.5 mm. Then, all the tunnel walls were metallized using copper tape. The input and output lines were connected to standard SMA connectors. The final circuits are shown in Figure 6. All simulations consider lossless materials and were performed using [13].

The final simulated and experimental results of the 2-pole filter are shown in Figure 7(a). The center frequency for the simulation and experiment is 3.6 GHz. Moreover, the return losses are better than 15 dB throughout the band for the experiment and better than 20 dB for the simulation. The experimental insertion losses are about 1 dB. The measured experimental BW is about 13%. This small difference can be attributed to the exclusion of losses in the simulation.

The final simulated and experimental results of the 3-pole filter are shown in Figure 7(b). The center frequency for the simulation and experiment is about 3.5 GHz. Moreover, the return losses are better than 14 dB throughout the band for the experiment and better than 16 dB for the simulation. The experimental insertion losses are about 1.3 dB. The experimental BW is about 14%, slightly wider than the simulation (13%).

The responses for the quasi elliptic filter are shown in Figure 8. Simulated and measured return losses are 15 dB and 13 dB, respectively. The experimental insertion losses are about 2.3 dB. From the figure, it is clear that the transmission zeroes are formed at 3.05 GHz and 4.2GHz for the simulation. For the experiment, they are located at 3.27 GHz and 3.99 GHz. The experimental BW is 10% compared with 13% for the simulation. This is attributed to the frequency shift of the hairpin resonators due to which forces transmission zeroes to be closer to the center frequency due to manufacturing tolerances.

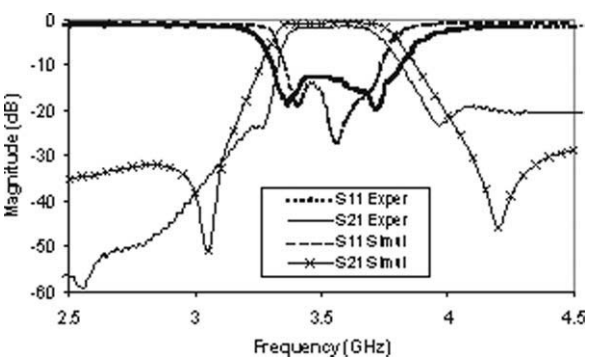

Figure 8 Simulated and measured reflection and transmission coefficients of quasi-elliptic filter

The small variations between simulation and experiment are due to fabrication errors, material tolerances, and material losses. However, good agreement is observed between experiment and simulation.

6. CONCLUSIONS

ENZ tunnels have been presented for their utilization in microwave filters. Two filters with Chebyshev responses and one quasi-elliptic response were successfully demonstrated in which simulated and experimental responses have reasonable agreement.

REFERENCES

1. B. Edwards, A. Alù, M.E. Young, M.G. Silveirinha, and N. Engheta, Experimental verification of epsilon-near-zero metamaterial coupling and energy squeezing using a microwave waveguide, Phys Rev Lett 100 (2008), 033903-1–033903-4.
2. M.G. Silveirinha and N. Engheta, Tunneling of electromagnetic energy through sub-wavelength channels and bends using epsilon-near-zero (ENZ) materials, Phys Rev Lett 97 (2006), 157403-1–157403-4.
3. B. Edwards, A. Alù, M.G. Silveirinha, and N. Engheta, Reflectionless sharp bends and corners in waveguides using epsilon-near-zero effects, J Appl Phys 105 (2009), 044905-1–044905-4.
4. A. Alu and N. Engheta, Antenna matching in ε-near-zero metamaterial channels, IEEE International Workshop on Antenna Technology, 2009. iWAT 2009, March 2–4, 2009.
5. A. Alu and N. Engheta, Dielectric sensing in ε-near-zero narrow waveguide channels, Phys Rev B 78 (2008), 045102-1–045102-5.
6. D.V.B. Murthy, A. Corona-Chavez, and J.L. Olvera-Cervantes, A novel epsilon near zero (ENZ) tunneling circuit using microstrip technology for high integrability applications, Prog Electromagn Res C 15 (2010), 6574.
7. A. Sanada, C. Caloz, and T. Itoh, Characteristics of the composite right/left-handed transmission lines, IEEE Microw Wireless Compon Lett 14 (2004), 68–70.
8. A. Sanada, C. Caloz, and T. Itoh, Zeroth order resonance in composite right/left-handed transmission line resonators, Asia-Pacific Microwave Conference, Seoul, Korea, Nov. 2003.
9. D.H. Shin and T. Itoh, A note on radiation loss of zeroth order resonators, Prog Electromagn Res C, 2 (2008), 109–116.
10. R. Liu, et al. experimental demonstration of electromagnetic tunneling through an epsilon-near-zero metamaterial at microwave frequencies, Phys Rev Lett 100 (2008), 023903.
11. W. Rotman, Plasma simulation by artificial dielectrics and parallel-plate media, IRE Trans Antennas Propag 10 (1962), 82–95.
12. R.E. Collin, Field theory of guided waves, 2nd ed., IEEE Press, New York, 1990.
13. Ansoft HFSS software, Pittsburgh, PA, version.11.

14. J.S. Hong and M.J. Lancaster, Microstrip filters for RF/microwave applications, Wiley, New York, NY, 2001.
15. Y. Li, M.J. Lancaster, F. Huang, and N. Roddis, Superconducting microstrip wide band filter for radio astronomy, International Microwave Symposium Digest, IEEE MTT-S, Philadelphia, PA, 2003, pp. 551–554.
16. R.R. Mansour, RF filters and diplexers for wireless system applications: state of the art and trends, Proceedings of the Radio and Wireless Conference, 2003. RAWCON '03.
17. G. Matthaei, L. Young, and E.M.T Jones, Microwave filters, impedance matching networks and coupling structures, Artech House, Norwood, MA, 1980.
18. K. Yeo, M.J. Lancaster, and J.S. Hong, The design of microstrip six-pole quasi-elliptic filter with linear phase response using extracted-pole technique, IEEE Trans Microwave Theory Tech 49 (2001), 321–327.

TUNABLE MICROWAVE PHOTONIC FREQUENCIES GENERATION BASED ON STIMULATED BRILLOUIN SCATTERING OPERATING IN THE L-BAND REGION

Harith Ahmad,[1] Siti Fatimah Norizan,[1] Noor Azura Awang,[1] M. Z. Zulkifli,[1] Z. A. Ghani,[2] and Sulaiman Wadi Harun[3]

[1] Photonics Laboratory, Department of Physics, University of Malaya, 5060 Kuala Lumpur, Malaysia; Corresponding author: harith@um.edu.my
[2] Faculty of Applied Sciences, Mara University of Technology, 40450 Shah Alam Selangor, Malaysia
[3] Department of Electrical Engineering, Faculty of Engineering, University of Malaya, 50603 Kuala Lumpur, Malaysia

Received 3 November 2010

ABSTRACT: *A tunable up frequencies of microwave photonics based on stimulated Brillouin scattering (SBS) for application in radio over fiber is demonstrated. The experimental setup consists of 7.7 km dispersion compensated fiber, which acts as the nonlinear medium for generating the SBS and is pumped by a narrow linewidth (0.015 nm) tunable laser operating in L-band region. The input-modulated RF at 2 GHz is upshifted to new frequencies of 7.71, 7.68, 7.65, 7.62, 7.58, and 7.56 GHz at Brillouin pump wavelengths of 1580, 1585, 1590, 1595, 1600, and 1605 nm, respectively. This system allows certain tunability in the upshifted frequencies by using a tunable laser source.* © 2011 Wiley Periodicals, Inc. Microwave Opt Technol Lett 53:1710–1713, 2011; View this article online at wileyonlinelibrary.com. DOI 10.1002/mop.26106

Key words: *fiber laser; stimulated Brillouin scattering; L-band region; microwave photonics*

1. INTRODUCTION

For a wireless network system, there is a need to improve on the transporting of the microwave frequency over a longer distance. One possible way is to transport the radio frequency (RF) over an optical fiber (RoF). This is an effective solution, because it provides low transmission losses that are achievable in a single-mode optical fiber. In fact, RoF has initiated considerable interests in recent years [1–3]. Generally, existing systems consist of base antenna station, which is connected to the center station through optical fibers. The signals are transmitted over the optical fiber at high frequencies, which requires high-frequency microwave generators, modulator, and high-speed photodetectors, which can be rather expensive. There are, however, other techniques that are based on nonlinear phenomenon in optoelectronics devices [4, 5]. There are also the optical methods, which are based on phase to intensity conversion in chip fiber gratings [6]. These methods are rather involved and an approach based on all optical technique will be an interesting option. There have been earlier reports using stimulated Brillouin scattering (SBS) in generating the up and down conversion of the RF signals in an optical fiber [7, 8], where two lasers are used with optical frequency locking system, which adds to the complexity in implementing the technique.

An improvement to this is to use a single laser, using SBS to up and down convert the RF signal and using fiber bandgap (FBGs) to simplify the process [9, 10]. The demonstrations are around the C-band region of the optical transmission spectrum and are limited to single input wavelength of a distributed feedback laser (DFB).

In this article, we report for the first time using a tunable laser, which is readily available at low cost, whereby the signal wavelengths in the L-band region be tuned to generate a tunable frequency upshifted signals. This method is also applicable for down conversion, which, due to limited facility, cannot be demonstrated in this article. The current technique allows flexibility in a system, and the L-band signals can be dedicated for the RF over fiber without interfering with existing optical traffics in the C-band region.

2. EXPERIMENTAL SETUP

The experimental set-up for microwave photonics frequency conversion utilizing the SBS in L-band region is shown in Figure 1. It consists of a Brillouin pump (BP), which is from a tunable laser source (Santec- MLS 2100) with the output power of 6 dBm and a linewidth of 0.015 nm, which is an important requirement for generating the SBS in a dispersion compensated fiber (DCF) of length 7.7 km and with effective core area of 15 μm^2. As the BP signals need to be modulated at 2 GHz, a Mach Zehnder modulator (MZM) is used. Normally, the insertion loss of a modulator can be relatively high, and in this case is about 7 dB. An optical amplifier is used to overcome this insertion loss. The optical amplifier consists of a bismuth-based erbium-doped fiber (Bi:EDF) with a length of 215 cm and a dopant concentration of 6300 ppm (Asahi Glass). It is set to provide a gain bandwidth of 50 nm centered on 1585 nm. The amplifier is bidirectionally pumped using two 1480-nm laser diodes with pumped power set to generate enough gain to compensate for the loss of power due to the MZM. The amplifier is set to operate with a gain of 12 dB for input signal of 0 dBm at a wavelength of 1560 nm. This Bi-EDF amplifier will boost up the BP to 12 dBm at its output end. The BP signal is connected to Port 1 of the optical circulator (OC) and exits at Port 2, which then enters the DCF through a fused coupler (1480/1550). The DCF is also pumped using another 1480-nm laser diode at 350 mW, which acts as the Raman pump. This generates a Raman fiber amplifier (RFA) with the DCF as the gain medium. This RFA will then amplify the BP with a net gain of 5 dB providing a BP output power of 17 dBm. The interaction of the BP and the DCF will create a backward Stokes labeled as first Stoke, which is down shifted to a new frequency given by the equation below,

$$f_s = 2n\upsilon_A/\lambda_p \tag{1}$$

where, n is the core refractive index of the DCF, υ_A is the acoustic wave velocity generated in the fiber, and λ_p is the BP wavelength. There is a minimum power requirement to generate the first Stoke and this is given by Eq. (2) [9] as,

$$P_{th} = \frac{21\,A_{eff}}{g_B(\nu_B)\,L_{eff}}\left[1 + \frac{\Delta\nu_p}{\Delta\nu_B}\right] \tag{2}$$